Energy & Environmental Science

PAPER

View Article Online
View Journal | View Issue

Cite this: *Energy Environ. Sci.*, 2014, **7**, 1142

Sub-150 °C processed meso-superstructured perovskite solar cells with enhanced efficiency†

Konrad Wojciechowski, Michael Saliba, Tomas Leijtens, Antonio Abate and Henry J. Snaith*

Received 12th November 2013
Accepted 23rd December 2013

DOI: 10.1039/c3ee43707h

www.rsc.org/ees

The ability to process amorphous or polycrystalline solar cells at low temperature (<150 °C) opens many possibilities for substrate choice and monolithic multijunction solar cell fabrication. Organometal trihalide perovskite solar cells have evolved rapidly over the last two years, and the $CH_3NH_3PbX_3$ (X = Cl, I or Br) material is processed at low temperature. However the first embodiments of the solar cell were composed of high temperature processed (500 °C) compact and mesoporous layers of TiO_2. The sintering of the mesoporous TiO_2 has been negated by replacing this with a mesoporous insulating scaffold in the meso-superstructured solar cell (MSSC), yet the high temperature processed compact TiO_2 layer still persists in the most efficient devices. Here we have realised a low temperature route for compact TiO_2, tailored for perovskite MSSC operation. With our optimized formulation we demonstrate full sun solar power conversion efficiencies of up to 15.9% in an all low temperature processed solar cell.

Broader context

Recent rapid development of organolead trihalide perovskite-based solar cells opens an attractive route for the realization of a much cheap alternative to today's commercially available solar technologies. The ultimate lowest cost and most versatile method of manufacture should be solution based low temperature processing. The low temperature aspect enables a broad range of substrates to be used for the solar cells, with potential applications ranging from space to light weight portable power with form factor, in addition to high throughput manufacture. Perovskite semiconductors are a perfect candidate to fulfil these needs thanks to their low cost, solution-processability and excellent optoelectronic properties. Until now, however, the most efficient solar cells have employed 500 °C sintered TiO_2 compact layers as charge selective contacts. Here, we have developed a low temperature processing route for compact TiO_2 films, which surpass the properties and subsequent performance in the perovskite solar cells, in comparison with the previous high temperature processed material. This finally removes all the sintering steps in the highest efficiency perovskite solar cells.

1. Introduction

Lightweight and mechanically flexible photovoltaic devices are of increasing interest and demand, mainly due to their ease of integration and versatile functionality. Potential applications range from portable electronic devices, electronic textiles, synthetic skin, robotics, and aerospace technology to large scale industrial roofing.[1–5] Commercially attractive reel-to-reel processing is contingent on low temperature technology in order to fabricate devices on the cheapest deformable flexible substrates, such as polyethylene terephthalate (PET) and polyethylene naphthalate (PFN). Additionally, low temperature fabrication allows for the possibility of new multi-junction device architectures, as it has been a successful route for higher efficiencies for organic photovoltaics,[6] and the highest efficiency crystalline photovoltaic technologies.[7] A recently emerged class of solution-processed hybrid solar cells are based on organometal trihalide perovskite absorbers, which exhibit exceptional performance[8–11] and are already approaching the performances of the best thin film technologies.[12,13] This cell type has been shown to work without high temperature sintering steps for the mesoporous scaffold,[11] closing the gap to achieve fully low-temperature solution-based manufacture. Recently, there have been a few reports of low temperature processed perovskite solar cells employing all organic p and n-type contacts.[14–16] However, for both the planar heterojunction and mesosuperstructured solar cells, the highest efficiency devices still require sintering of the TiO_2 compact layer, working as a selective contact for electron collection at the anode.[17] Typically, this compact layer is prepared by spin-coating or spray pyrolysis of a solution of TiO_2 precursor with subsequent sintering at 500 °C in order to transform the amorphous oxide layer into the crystalline form (anatase), which provides good charge transport properties. The problem of high temperature processing of the TiO_2 compact layer has been addressed previously for dye-sensitized solar cells (DSSCs): atomic layer

Department of Physics, University of Oxford, Clarendon Laboratory, Parks Road, Oxford OX1 3PU, UK. E-mail: h.snaith1@physics.ox.ac.uk

† Electronic supplementary information (ESI) available: Additional SEM images, photovoltaic performance parameters and recombination lifetime with a description of photovoltage and photocurrent decay measurements. See DOI: 10.1039/c3ee43707h

deposition,[18,19] microwave sintering[20] and inductively coupled plasma (ICP)-assisted DC magnetron sputtering[21] have been used for deposition. However, the results generally yield lower efficiency in DSSCs than high-temperature processed TiO_2. Here we report a low temperature fabrication (<150 °C) of a compact layer composed of highly crystalline small nanoparticles of anatase TiO_2 (diameter <5 nm) dispersed in an alcoholic solvent with an addition of titanium diisopropoxide bis(acetylacetonate) (TiAcAc). This approach results in a dense TiO_2 layer with up to 100 fold higher conductivity than the TiO_2 produced from the previous high temperature route. The ensuing all-low-temperature processed MSSC outperforms the previous state-of-the-art devices, delivering a maximum full sun power conversion efficiency of 15.9%.

2. Results and discussion

In this work, we compare the newly developed TiO_2 compact layer, which we term low temperature TiO_2 (lt-TiO_2), with the standard recipe used in MSSCs in which a solution of titanium isopropoxide in acidic ethanol is spin-coated upon the substrate.[11] For the conventional route, we either dry the films at 150 °C (which we term amorphous TiO_x) or sinter the films at 500 °C as is done in the current state-of-the-art (which we term high temperature (ht)-TiO_2) devices. Here, we synthesize TiO_2 nanoparticles by a nonaqueous route from titanium tetrachloride and benzyl alcohol,[22] the detailed procedure is described in the Experimental section. In Fig. 1c we show the X-ray diffraction (XRD) spectrum of a powdered sample, which can be assigned to anatase TiO_2 with a crystal diameter of approximately 4.5 nm, as determined by Scherrer peak width analysis.[23]

Elsewhere, we have shown that adding TiAcAc to TiO_2 mesoporous single crystals can greatly enhance the adhesive properties of the film and enhance the operation of dye-sensitized solar cells when processed at low temperature.[24] Here, we added a small amount of TiAcAc (initially 10 mol% with respect to the TiO_2 content) to the colloidal TiO_2 dispersion, prior to spin-coating and drying at 150 °C. We propose that the TiAcAc decomposes to TiO_x during film drying and bridges the gaps between the nanoparticles; otherwise put, it creates the mortar to hold the nanoparticles together.[25] We observed that an opaque dispersion of TiO_2 becomes translucent a few hours after TiAcAc addition, which we attribute to the chelation of acetylacetonate ligands to the TiO_2 nanoparticles.[26] We show SEM images of the spin-coated lt-TiO_2 films in Fig. 1a and b and S1a–c,† which exhibit "crack free" uniform continuous coverage of the substrates.

We investigated the impact of varying the concentration of TiAcAc from 0 to 80 mol% with respect to TiO_2 upon the conductivity of the films, and compared them to the standard fabricated TiO_2 films. The results that we show in Table 1 demonstrate that TiO_x is the least conductive (2×10^{-6} S cm^{-1}), an order of magnitude lower than the conventional ht-TiO_2. Remarkably, even the TiO_2 sol shows a 50-fold increase in conductivity over the ht-TiO_2 and with the addition of a small amount of TiAcAc this increases to a maximum of just below 10^{-3} S cm^{-1}. This demonstrates that at least as far as the conductivity and hence series resistance are concerned, the new low temperature TiO_2 compact layer should be better than the previous state-of-the-art sintered compact layer devices. However, if we calculate the equivalent series resistance for current flowing perpendicularly through a 1 cm^2 slab of 50 nm thick material, as we also show in Table 1, only the TiO_x should contribute significantly to the solar cells' series resistance.

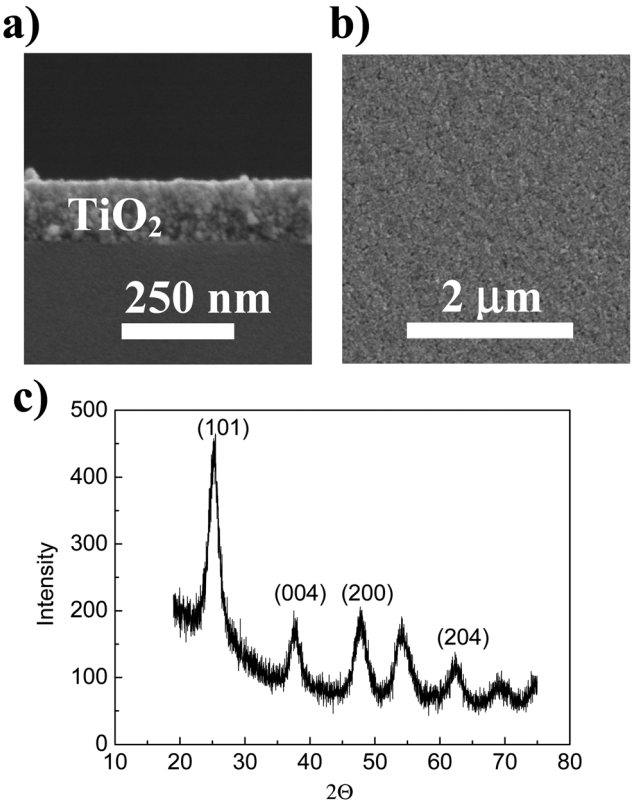

Fig. 1 (a) Cross-sectional image of 3.54 weight% TiO_2 NPs spin-coated on glass, thickness: 100–120 nm; (b) top surface image of lt-TiO_2; (c) X-ray diffraction spectrum of the TiO_2 nanoparticle powder sample.

We incorporated these TiO_2 compact layers into complete MSSCs and present the current–voltage curves in Fig. S1.† The optimum concentration for performance was 20 mol% TiAcAc, which we use for the rest of the study. We then varied the thickness of the compact TiO_2 films by varying the TiO_2 sol concentration. We present the photovoltaic performance parameters for devices with the range of compact layer thicknesses in Fig. S2,† where we found the optimum thickness to be approximately 45 nm.

In Fig. 2 we present solar cell current voltage curves and performance parameters by comparing the best performing MSSC fabricated with the optimised low temperature processed TiO_2 formulation (lt-TiO_2) as compared to devices employing high temperature processed TiO_2 (ht-TiO_2) and amorphous TiO_x. We show the solar cell performance parameters, along with the solar cell series resistance determined by fitting the slope of the *J–V* curve near open-circuit in Table 2. Devices with the optimum low temperature processed compact layer surpass the performance of the previous state-of-the-art sintered

Table 1 Conductivity values of different blocking layers

Blocking layer	Conductivity (S cm^{-1})	Calculated resistance through 50 nm thick film (Ω cm^2)
TiO_x	0.02×10^{-4}	2.500
Ht-TiO_2	0.11×10^{-4}	0.455
Lt-TiO_2 (0 mol% TiAcAc)	5.08×10^{-4}	0.010
Lt-TiO_2 (10 mol% TiAcAc)	8.32×10^{-4}	0.006
Lt-TiO_2 (20 mol% TiAcAc)	6.80×10^{-4}	0.007
Lt-TiO_2 (40 mol% TiAcAc)	4.15×10^{-4}	0.012
Lt-TiO_2 (80 mol% TiAcAc)	0.24×10^{-4}	0.208
Spiro-OMeTAD (250 nm)	0.30×10^{-4}	0.833

compact layer devices, delivering a maximum power conversion efficiency of 15.3%. The improvement is mainly due to higher fill factor, which rises above 0.7 in the best devices, consistent with reduced overall series resistance in the solar cell. Following from this work, we re-optimized the perovskite precursor concentration in the spin-coated solution (see the Experimental section) and achieved further increase in the film thickness, and overall performance of the solar cells, delivering a maximum full sun power conversion efficiency of 15.9%, with an average of 14.7%. The increased performance arises from the average increase in the short-circuit photocurrent. We present the statistical distribution of the photovoltaic parameters of the optimised batch (ht-TiO_2 *vs.* lt-TiO_2) in Fig. S4.†

The new low temperature processed compact TiO_2 has higher conductivity than the previously sintered material, and the ensuing solar cells have characteristics of lower overall series resistance. Fortuitously, this is not offset by faster recombination (which we show in the ESI†) or a less favourable band offset, which we infer from the relative invariance in the open-circuit voltage. At first sight the reduced series resistance in the solar cell is surprising, since the ht-TiO_2 should have only been contributing on the order of 0.5 Ω cm^2 to the solar cell series resistance. In addition, we have previously reasoned for solid-state dye-sensitized solar cells that the series resistance at open-circuit is limited by hole-conduction through spiro-OMeTAD.[27] However, here the spiro-OMeTAD is simply a solid

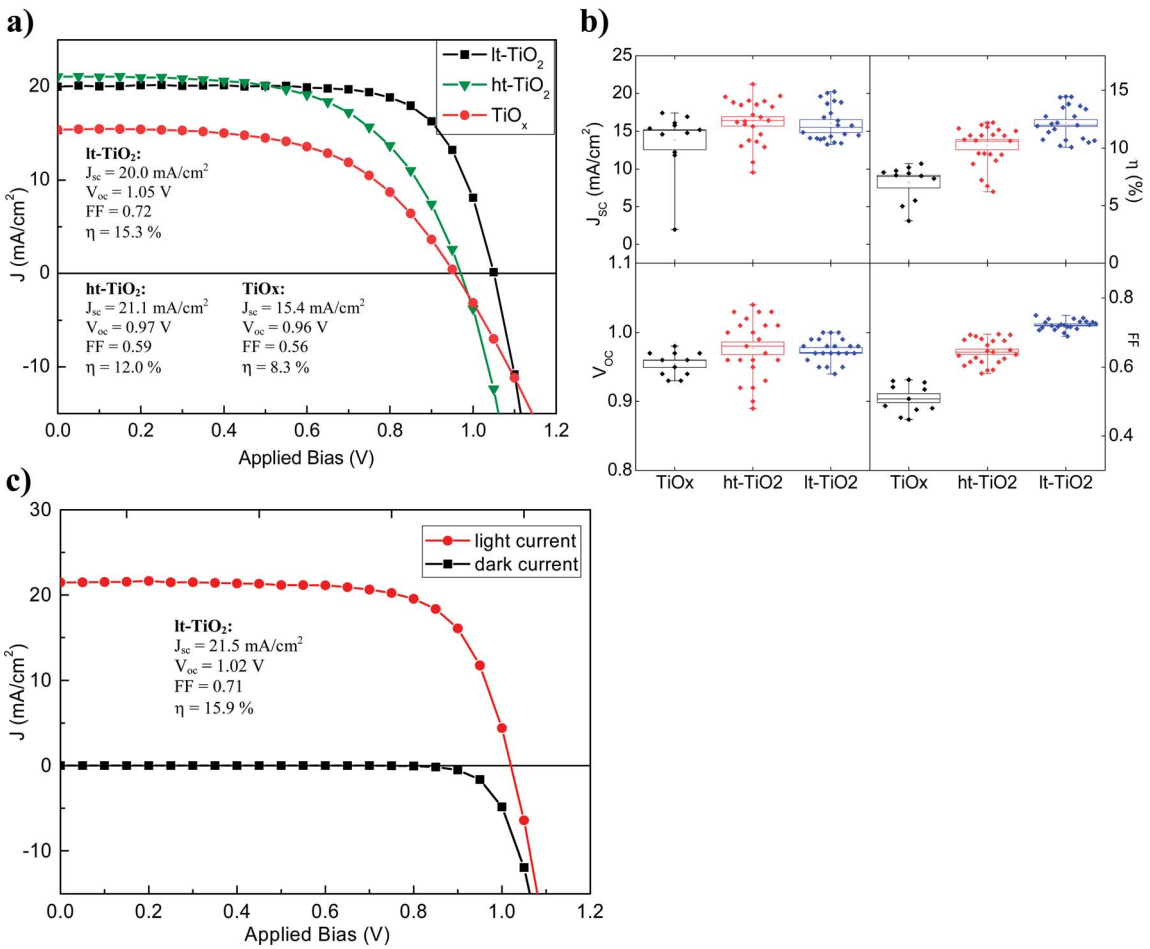

Fig. 2 (a) Current–voltage characteristics of the best performing solar cells prepared using amorphous (TiO_x), high-temperature (ht-TiO_2) and low-temperature (lt-TiO_2) processed compact layers; (b) photovoltaic parameters extracted from current–voltage measurements of a series of solar cells with different compact layers; (c) record lt-TiO_2 solar cell performance obtained by increasing the perovskite film thickness.

Table 2 Photovoltaic parameters extracted from current–voltage measurements of devices with different compact layers

Compact layer (mean ± s.d.)	J_{sc} (mA cm^{-2})	η (%)	V_{OC} (V)	FF	R_s (Ω cm^2)
TiO_x	13.85 ± 4.30	7.03 ± 1.59	0.95 ± 0.02	0.51 ± 0.04	18.93 ± 4.87
Ht-TiO_2	16.33 ± 2.98	10.22 ± 1.74	0.98 ± 0.04	0.64 ± 0.04	9.22 ± 1.19
Lt-TiO_2 (20 mol% TiAcAc)	16.06 ± 2.37	12.18 ± 1.46	0.97 ± 0.02	0.72 ± 0.01	6.12 ± 0.88

capping layer (~250 nm thick as opposed to 2 μm infiltrated into a porous medium in the dye-sensitized solar cells) with a conductivity of close to 3×10^{-5} S cm^{-1}.[27,28] Hence the overall series resistance expected through a 250 nm thick film of doped spiro-OMeTAD is only 0.8 Ω cm^2. However, the overall series resistances of the devices are much higher than the sum of bulk resistances of the compact layer and hole transporter (see Tables 1 and 2), and the difference between the devices incorporating lt-TiO_2 and ht-TiO_2 is over 3 Ω cm^2. Some of the extra resistance could arise from contact resistance, either present at the perovskite/TiO_2 or the TiO_2/FTO contacts. In particular, there is prior evidence for a potential barrier present at the FTO/TiO_2 interface.[29–31] *Via* Mott–Schottky analysis, the donor density in conventional high temperature processed compact layers employed in dye-sensitized solar cells is in the order of 10^{19} cm^{-3}.[32] Assuming a dielectric of 100 for the TiO_2, a space charge depletion width, W, can be calculated using,[32]

$$W = \sqrt{\frac{2\varepsilon\varepsilon_0(E - E_{fb})}{eN}} \quad (1)$$

where N is the concentration of electron donors, ε is the TiO_2 dielectric constant, ε_0 is the vacuum permittivity and E_{fb} is the flat-band potential. $E - E_{fb}$ is approximately the difference between the FTO work function (−4.4 eV)[33] and the Fermi-level in TiO_2 (the latter of which should be higher (deeper) than the conduction band edge of TiO_2 at −4.1 eV).[34] With a charge density of 10^{19} cm^{-3}, we estimate a depletion width of approximately 20 nm. This is in the order of the film thickness employed for our optimum compact layers, which implies that band bending appears to be appropriate. However, it also implies that significant depletion throughout the compact layer could occur for the thinnest films, greatly increasing the bulk series resistance beyond that measured from the isolated films on glass. For the low temperature TiO_2 here, the conductivity is between 10 and 100 times greater than both the high temperature films presented here and those fabricated by spray pyrolysis deposition.[32] If this increase in conductivity is largely due to an increase in the donor density, then with a donor density of 10^{20}, the depletion width would reduce to 6 nm. In this instance the film would not be completely depleted giving much higher bulk conductivity, and additionally the narrower barrier width should enable a lower contact resistance. We note that heavily doping semiconductors at semiconductor-metal contacts is routine to minimise the contact resistance.[35]

To probe the origin of the reduced series of the lt-TiO_2 devices in more detail, we have performed small perturbation transient photovoltage and photocurrent decay measurements, from which we can determine the differential capacitance of the solar cell.[36] This is usually employed to probe the chemical capacitance of mesoporous TiO_2, with the differential capacitance being interpreted to reflect the density of states in the tail of the TiO_2 conduction band. Here, we are using it to probe any changes which may have been introduced due to the different compact TiO_2 layers. In Fig. 3 we show that the differential capacitance as a function of open-circuit voltage is considerably different for the devices with different compact layers. This is quite surprising, since we would assume the chemical capacitance of such a thin film of TiO_2 to be very low. Devices with ht-TiO_2 show much broader distribution of states than cells with lt-TiO_2, suggesting significant reduction in sub-band gap states in the low temperature processed films, or that the sub-bandgap states are predominantly filled in the lt-TiO_2, consistent with the enhanced conductivity. Alternatively, the capacitance could be due to the depletion of the compact TiO_2 at the FTO interface, which as discussed above, will lead to a considerably broader depletion region in the ht-TiO_2 than the lt-TiO_2 films. In addition, capacitance which may be present due to accumulation or depletion within the perovskite at the perovskite/TiO_2 interface may also contribute. We note that although these measurements and rationale indicate that a potential barrier at the FTO–TiO_2 interface could contribute to the series resistance in the solar cell, further investigations are required to understand in much more detail the electronic structure across the FTO–TiO_2 and TiO_2-perovskite heterojunctions.

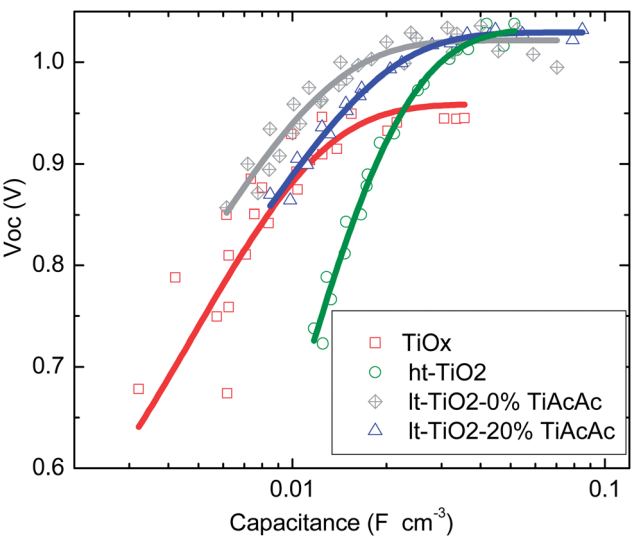

Fig. 3 Open circuit voltage against the differential capacitance.

3. Conclusions

In summary, we have successfully developed a route for creating a low temperature processed TiO_2 compact layer and in doing so we have finally removed all the high temperature thermal processing steps for the mesosuperstructured and planar heterojunction perovskite solar cells. Through this work, we have discovered that the previously employed high temperature processed compact TiO_2 layer was contributing significantly to the series resistance of the solar cells. The new low temperature approach has hence additionally resulted in improved fill factors and efficiency, pushing the solution processed MSSC back to the very highest efficiencies for perovskite solar cells. This work now makes the MSSC compatible with polymer foil flexible substrates and opens the door for monolithic multi-junction perovskite solar cells.

4. Experimental

Unless otherwise stated, all materials were purchased from Sigma-Aldrich or Alfa Aesar and used as received. Spiro-OMeTAD was purchased from Borun Chemicals and used as received. The synthesis of the perovskite $CH_3NH_3PbI_{3-x}Cl_x$ has been reported elsewhere.[10] TiO_2 nanoparticles were synthesized following a previously reported method.[22] In a typical synthesis 2 ml of anhydrous $TiCl_4$ (99.9%) was added dropwise while stirring into a vial containing 8 ml of anhydrous ethanol. The whole content was transferred into a 100 ml flask containing 40 ml anhydrous benzyl alcohol. The solution was heated to 80 °C and reacted for 9 hours. After that time the reaction was stopped by cooling down the solution, which contained a translucent dispersion of very fine TiO_2 nanoparticles. Then, 4 ml of the above solution was mixed with 36 ml of diethyl ether resulting in the precipitation of the TiO_2. The precipitate was centrifuged, washed with acetone and redispersed in anhydrous ethanol, resulting in a colloidal solution of approximately 28 mg TiO_2/ml ethanol (3.54 wt% of TiO_2). The formulation was further diluted 3 times (1.18 wt% of TiO_2) in anhydrous ethanol and the appropriate amount of TiAcAc (10–20 mol% with respect to the TiO_2 content) was added directly. The solution was left to stand for at least 2 hours before use, but is stable for months. The low temperature TiO_2 compact layer (lt-TiO_2) was prepared by spin-coating the colloidal dispersion of anatase particles in anhydrous ethanol, formulated with TiAcAc, followed by drying at 150 °C for 30 minutes. The thickness of the compact layer was tuned by the concentration of TiO_2 nanoparticles (3.54–0.24 wt% TiO_2 to ethanol). As standard control samples, blocking layers of non-crystalline TiO_x and high temperature processed TiO_2 (ht-TiO_2) were used. The former was prepared by spin-coating a precursor solution (titanium isopropoxide, TTIP) in anhydrous ethanol (0.254 M) with the addition of 0.02 M HCl followed by annealing at 150 °C for 30 min, the latter was prepared by spin-coating the same solution (TTIP), followed by annealing at 150 °C and sintering at 500 °C.

Photovoltaic devices were fabricated on fluorine-doped tin oxide (FTO) coated glass (Pilkington, TEC7). Substrates were cleaned in hallmanex, and then subjected to 10 minutes sonication in acetone, 10 minutes sonication in IPA, and 10 minutes of oxygen plasma etching. Compact layers were deposited by spin-coating, as described above. An alumina scaffold was deposited according to the previously reported method which employs Al_2O_3 nanoparticles of diameter <50 nm.[11] After depositing the alumina scaffold samples were transferred into a nitrogen-filled glovebox, initially optimised precursor solution of the concentration of 350 mg ml^{-1} (CH_3NH_3I and $PbCl_2$, 3 : 1 molar ratio in *N*,*N*-dimethylformamide (DMF)) was spin-coated at room temperature, followed by annealing at 100 °C for 90 minutes. The concentration of the precursor solution was re-optimised to 400 mg ml^{-1}, resulting in an increased perovskite film thickness. The hole transporter was deposited by spin-coating an 8 wt% 2,2′,7,7′-tetrakis-(*N*,*N*-di-*p*-methoxyphenylamine)9,9-spirobifluorene (spiro-OMeTAD) in chlorobenzene with added *tert*-butylpyridine (*t*BP) and lithium bis(trifluoromethanesulfonyl)imide (Li-TFSI) of 80 and 30 mol%, with respect to spiro-OMeTAD. Finally, 150 nm thick silver electrodes were deposited on top of devices by thermal evaporation at $\sim 10^{-6}$ bar, through a shadow mask.

4.1 Characterization techniques

UV-Vis absorption spectra were obtained using a Carry 300 Bio (Agilent Technologies) spectrometer. Scanning electron microscopy images were obtained using a Hitachi S-4300 microscope. Conductivity measurements of TiO_2 films were performed by evaporating gold electrodes through the shadow mask on the spin-coated compact layers and using a 4-point probe set up with a Keithley 2400 as a sourcemeter. The electrode pattern was designed for 4-point probe measurements with an outer probe channel dimensions of 1 mm (length) × 1 cm (width) and an inner probe separation of 300 μm. The thickness of the channel (TiO_2 layer) was determined from the SEM cross-sectional image. X-ray diffraction spectra were obtained for powder samples (the nanoparticle solution was dried in air at 150 °C) using a Panalytical X'Pert Pro X-ray diffractometer.

Current–voltage characteristics of solar cells were measured under simulated AM1.5 100 mW cm^2 sunlight (ABET Technologies Sun 2000) with a Keithley 2400 sourcemeter. The lamp was calibrated with an NREL-calibrated KG5 filtered silicon reference with a solar mismatch factor of 1.01. The active area of the device was defined by a metal mask with a square aperture of an area of 0.0625 cm^2. The pre-masked active area of the solar cells was approximately 0.12 cm^2 nominally defined by the overlap area of the silver and FTO electrodes. Solar cells were masked for all the current voltage measurements.

Acknowledgements

This work was supported by EPSRC, Oxford Photovoltaics Ltd. and the European Research Council (ERC) through the HYPER PROJECT no. 279881.

Notes and references

1 C. H. Lee, D. R. Kim, I. S. Cho, N. William, Q. Wang and X. Zheng, *Sci. Rep.*, 2012, **2**, 1000.
2 D. J. Lipomi and Z. Bao, *Energy Environ. Sci.*, 2011, **4**, 3314.
3 M. B. Schubert and J. H. Werner, *Mater. Today*, 2006, **9**, 42–50.
4 A. J. Baca, K. J. Yu, J. Xiao, S. Wang, J. Yoon, J. H. Ryu, D. Stevenson, R. G. Nuzzo, A. A. Rockett, Y. Huang and J. A. Rogers, *Energy Environ. Sci.*, 2010, **3**, 208.
5 M. Kaltenbrunner, M. S. White, E. D. Głowacki, T. Sekitani, T. Someya, N. S. Sariciftci and S. Bauer, *Nat. Commun.*, 2012, **3**, 770.
6 S. Esiner, H. van Eersel, M. M. Wienk and R. A. J. Janssen, *Adv. Mater.*, 2013, **25**, 2932–2936.
7 M. A. Green, K. Emery, Y. Hishikawa, W. Warta and E. D. Dunlop, *Progress in Photovoltaics: Research and Applications*, 2013, **21**, 827–837.
8 A. Kojima, K. Teshima, Y. Shirai and T. Miyasaka, *J. Am. Chem. Soc.*, 2009, **131**, 6050–6051.
9 H.-S. Kim, C.-R. Lee, J.-H. Im, K.-B. Lee, T. Moehl, A. Marchioro, S.-J. Moon, R. Humphry-Baker, J.-H. Yum, J. E. Moser, M. Grätzel and N.-G. Park, *Sci. Rep.*, 2012, **2**, 591.
10 M. M. Lee, J. Teuscher, T. Miyasaka, T. N. Murakami and J. Henry, *Science*, 2012, **338**, 643–647.
11 J. M. Ball, M. M. Lee, A. Hey and H. J. Snaith, *Energy Environ. Sci.*, 2013, **6**, 1739.
12 J. Burschka, N. Pellet, S.-J. Moon, R. Humphry-Baker, P. Gao, M. K. Nazeeruddin and M. Grätzel, *Nature*, 2013, **499**, 316–319.
13 M. Liu, M. B. Johnston and H. J. Snaith, *Nature*, 2013, **501**, 395–398.
14 J.-Y. Jeng, Y.-F. Chiang, M.-H. Lee, S.-R. Peng, T.-F. Guo, P. Chen and T.-C. Wen, *Adv. Mater.*, 2013, **25**, 3727–3732.
15 S. Sun, T. Salim, N. Mathews, M. Duchamp, C. Boothroyd, G. Xing, T. C. Sum and Y. M. Lam, *Energy Environ. Sci.*, 2014, **7**, 399.
16 P. Docampo, J. M. Ball, M. Darwich, G. E. Eperon and H. J. Snaith, *Nat. Commun.*, 2013, **4**, 2761.
17 B. Peng, G. Jungmann, C. Jäger, D. Haarer, H.-W. Schmidt and M. Thelakkat, *Coord. Chem. Rev.*, 2004, **248**, 1479–1489.
18 C. Y. Jiang, W. L. Koh, M. Y. Leung, S. Y. Chiam, J. S. Wu and J. Zhang, *Appl. Phys. Lett.*, 2012, **100**, 113901.
19 D. Muñoz-rojas, H. Sun, D. C. Iza, J. Weickert, L. Chen, H. Wang, L. Schmidt-mende and J. L. Macmanus-driscoll, *Progress in Photovoltaics: Research and Applications*, 2013, **21**, 393–400.
20 J. N. Hart, D. Menzies, Y.-B. Cheng, G. P. Simon and L. Spiccia, *J. Sol-Gel Sci. Technol.*, 2006, **40**, 45–54.
21 H.-J. Kim, J.-D. Jeon, D. Y. Kim, J.-J. Lee and S.-Y. Kwak, *J. Ind. Eng. Chem.*, 2012, **18**, 1807–1812.
22 J. Wang, J. Polleux, J. Lim and B. Dunn, *J. Phys. Chem. C*, 2007, **2**, 14925–14931.
23 L. Kavan, J. Procházka, T. M. Spitler, M. Kalbáč, M. Zukalová, T. Drezen and M. Grätzel, *J. Electrochem. Soc.*, 2003, **150**, A1000.
24 E. J. W. Crossland, N. Noel, V. Sivaram, T. Leijtens, J. A. Alexander-Webber and H. J. Snaith, *Nature*, 2013, **495**, 215–219.
25 J. M. Szeifert, D. Fattakhova-rohlfing, D. Georgiadou, V. Kalousek, J. Rathouský, D. Kuang, S. Wenger, S. M. Zakeeruddin, M. Gra and T. Bein, *Chem. Mater.*, 2009, **21**, 1260–1265.
26 H.-J. Chen, L. Wang and W.-Y. Chiu, *Mater. Chem. Phys.*, 2007, **101**, 12–19.
27 A. Abate, T. Leijtens, S. Pathak, J. Teuscher, R. Avolio, M. E. Errico, J. Kirkpatrik, J. M. Ball, P. Docampo, I. McPherson and H. J. Snaith, *Phys. Chem. Chem. Phys.*, 2013, **15**, 2572–2579.
28 T. Leijtens, J. Lim, J. Teuscher, T. Park and H. J. Snaith, *Adv. Mater.*, 2013, **25**, 3227–3233.
29 H. J. Snaith and M. Grätzel, *Adv. Mater.*, 2006, **18**, 1910–1914.
30 S. Ru and D. Cahen, *J. Phys. Chem. B*, 2004, **108**, 17946–17951.
31 S. Rühle and T. Dittrich, *J. Phys. Chem. B*, 2005, **109**, 9522–9526.
32 L. Kavan and M. Graetzel, *Electrochim. Acta*, 1995, **40**, 643–652.
33 A. Andersson, N. Johansson, P. Bröms, N. Yu, D. Lupo and W. R. Salaneck, *Adv. Mater.*, 1998, **10**, 859–863.
34 M. Grätzel, *Nature*, 2001, **414**, 338–344.
35 A. Y. C. Yu, *Solid-State Electron.*, 1970, **13**, 239–247.
36 P. Docampo, S. Guldin, M. Stefik, P. Tiwana, M. C. Orilall, S. Hüttner, H. Sai, U. Wiesner, U. Steiner and H. J. Snaith, *Adv. Funct. Mater.*, 2010, **20**, 1787–1796.